"© 2020 IEEE. Personal use of this material is permitted. Permission from IEEE must be obtained for all other uses, in any current or future media, including reprinting/republishing this material for advertising or promotional purposes, creating new collective works, for resale or redistribution to servers or lists, or reuse of any copyrighted component of this work in other works."

High Directivity, Compact, Omnidirectional Horizontally Polarized Antenna Array

Wei Lin, *Senior Member, IEEE* and Richard W. Ziolkowski, *Life Fellow, IEEE*

***Abstract*—Omnidirectional horizontally polarized (OHP) X-band magnetic dipole antenna arrays are reported that simultaneously achieve high directivity and wide bandwidth while being compact in size. A major innovation is the seamless integration of several phase inverters into an electrically long $TE_{0.5,0}$ mode open waveguide. The resulting open structure radiates as a collinear series of magnetic dipole sections. The inverters facilitate the realization of in-phase electric fields along its entire length and, hence, phase coherence between all of these magnetic dipoles. Each phase inverter is realized as a combination of a meandering slot on one metallic surface of the waveguide and several shorting vias surrounding it. Two such multi-staged (six- and eight-element) collinear OHP magnetic dipole arrays were designed and optimized. Prototypes of both were fabricated with standard, low-cost PCB manufacturing technology. The volume of the six-element (eight-element) OHP array is only $0.07 \times 0.22 \times 3.3\ \lambda_0^3$ ($0.07 \times 0.22 \times 4.3\ \lambda_0^3$); it achieves a measured 8.2 dBi (10.4 dBi) peak realized gain. The measured overlapping -10-dB impedance and 3-dB realized gain bandwidth was 8% in both cases. These designs are ideal for wireless applications requiring thin high directivity HP sources covering the entire azimuthal plane.**

***Index Terms*—Antenna array, compact, high directivity, horizontal polarization, magnetic radiators, omnidirectional radiation, phase inverter.**

I. Introduction

OMNIDIRECTIONAL antennas have been widely used in wireless communication applications because of their large radiation coverage areas, e.g., in indoor wireless local area network (WLAN), outdoor TV broadcasting and device-to-device (D2D) communication systems [1] – [4]. In particular, omnidirectional horizontally polarized (OHP) antennas have drawn much recent attention due to the desire for polarization diversity with respect to commonly employed vertically polarized (VP) antennas. Combinations of orthogonal OHP and OVP antennas can increase the system capacity as well as mitigate polarization mismatch effects in multipath environments [5]. Moreover, horizontally polarized systems have achieved 10 dB more received power than VP systems in indoor multipath environments [6]. Thus, compact and highly efficient OHP antennas and arrays are commercially attractive and, hence, highly desired.

Manuscript received on 22nd October 2019, revised on 27th February 2020.

Wei Lin and Richard. W. Ziolkowski are with the University of Technology Sydney, Global Big Data Technologies Centre, Ultimo NSW 2007, Australia, (E-mail: wei.lin@uts.edu.au).

Many OHP antennas have been investigated to date [7] – [25]. Their design methodologies can be summarized simply into two categories: either radiating slots or current loops. For instance, slots as magnetic radiators that achieved OHP radiation were developed successfully in [7], [8]. Many more efforts have focused on the development of OHP radiating loop designs. Examples include the original Alford loop [9] and its modifications [10] – [12]; segmented loops [13] – [16]; cross dipoles [17] – [19]; and multiple curved dipoles excited by feed networks [20] – [25]. All of these OHP antenna designs realize a single magnetic dipole radiator with low directivity. It has remained a challenge to develop a high directivity OHP antenna array that simultaneously is compact in size, has an acceptable bandwidth and is a compact structure that is easy to fabricate.

One approach to design a high directivity OHP antenna array is to construct a collinear set of magnetic elements, e.g., slots that radiate in-phase. For example, a five-element collinear magnetic dipole array was realized in [26] as a set of half-enclosed rectangular cavities whose radiating apertures are excited with a center-fed parallel strip line. A high directivity OHP pattern was observed with a peak realized gain value of 8.64 dBi. However, the operating bandwidth was only 2%. Substrate integrated waveguide (SIW) based slot antenna arrays have realized high directivity OHP radiation [27], [28]. Nevertheless, the achieved bandwidths were again narrow, less than 3.6%, and did not completely cover the intended WLAN application bandwidth, which is 4.1% from 2.4 to 2.5 GHz. On the other hand, a microstrip magnetic dipole array based on an open waveguide has achieved OHP radiation with a 7.3% bandwidth and a 9.7 dBi peak realized gain [29]. The total length $6\lambda_0$, however, is long.

Yet another magnetic radiator approach to realize high directivity OHP radiation is to excite a set of collinear radiating loops with an external feed network. It improves the bandwidth effectively. For instance, an OHP array was realized by exciting four mu-negative transmission line (MNG-TL) loop antennas with a feed network [30]. A wide 10.6% bandwidth and a high 8.7 dBi omni-directivity were obtained. Nevertheless, the volume of this cylindrical structure, $\pi\,(0.38)^2 \times 2\,\lambda_0^3 = 0.91\,\lambda_0^3$, is large. A second approach employed eight radiating loops that were collinearly excited with a 1 to 8 feed network to achieve the broad bandwidth of 34% [31]. Unfortunately, the loss (> 3 dB) from its complicated feed network is significant. Moreover, the peak realized gain was only 8 dBi given that the total volume was very large: $\pi\,(0.55)^2 \times 7.1\,\lambda_0^3 = 6.75\,\lambda_0^3$. A third approach has been to adopt leaky-wave structures [32], [33].

However, their beam angles are frequency-dependent and their lengths are long.

An innovative OHP antenna array design is introduced in this paper that simultaneously achieves a high directivity, is compact and easy to fabricate, and has a wide bandwidth. It is based on an electrically long $TE_{0.5,\,0}$ mode open rectangular waveguide and a set of seamlessly integrated phase inverters, each separated by a half wavelength. Each of the resulting half-wavelength sections acts as a magnetic radiator. Each phase inverter is realized as the combination of a meandering slot on the top metallic surface of the waveguide and several shorting vias that are distributed on both sides of the slot in an alternating pattern. These phase inverters facilitate having the electric fields be in-phase along the entire open aperture. Thus, a multiple-stage collinear magnetic dipole array is formed.

Two OHP antenna arrays based on this design paradigm are optimized, fabricated and tested. The first is a single-feed six-element OHP antenna array. Its volume is only $0.07 \times 0.22 \times 3.3\ \lambda_0^3 = 0.051\ \lambda_0^3$. The overlapping −10-dB impedance and 3-dB gain bandwidths cover 800 MHz from 9.6 to 10.4 GHz (8%) in the X-band. The peak realized omnidirectional gain is 8.2 dBi. The peak realized gain (RG) per unit wavelength is defined to quantify the directivity enhancement capability of the collinear omnidirectional antenna array, whose directivity is proportional to its total length. The RG per λ_0 of the six-element array is 2.48 dBi/λ_0. The second is a dual-feed eight-element OHP antenna array to further increase the peak realized gain. While achieving a peak realized gain of 10.4 dBi, it also maintained the overlapping bandwidth of 800 MHz from 9.6 to 10.4 GHz (8%). The total volume is only $0.07 \times 0.22 \times 4.3\ \lambda_0^3 = 0.066\ \lambda_0^3$ and the RG per λ_0 is 2.42 dBi/λ_0. The design paradigm leads to high performance OHP magnetic dipole arrays that are ideal candidates for many wireless applications including base station antennas for WLAN, vehicle to vehicle communications, and power sources for far field wireless power transfer applications [34].

The paper is organized as follows. Sec. II discusses the design approach. Sec. III presents the operating principles, design considerations, and the simulated and measured results of both prototypes. Conclusions are summarized in Sec. IV.

II. Design Paradigm

The realization of the OHP magnetic dipole array was originally inspired by the classic Franklin antenna [35]. The version depicted in Fig. 1(a) is an electrically long ($3\lambda_0$) dipole with folded sections to obtain in-phase collinear dipoles that radiate high directivity, vertically polarized, omnidirectional fields. The introduction of the folded stubs along the radiator eliminates the out-of-phase currents where they are located.

Analogously, the center-fed electrically long ($3\lambda_0$) $TE_{0.5,0}$ mode open waveguide (open on one long side only) in Fig. 1(b) forms six collinear half-wavelength magnetic dipoles (MDs). The detailed analysis demonstrating that a $TE_{0.5,0}$ mode open waveguide is equivalent to a magnetic dipole was reported in [29]. The phase of each MD changes 180° for every half wavelength distance from the feed point in the middle towards each end. As illustrated, four magnetic dipoles are in-phase (pointing right to left) and the remaining two are out-of-phase (pointing left to right). If the two out-of-phase magnetic dipoles were effectively suppressed or even better, brought into phase with the other four, a high directivity, HP, omnidirectional magnetic dipole array would be realized.

One approach to suppress the out-of-phase MDs is to short out the two sections of the $TM_{0.5,0}$ mode waveguide where the electric fields are out-of-phase. This is accomplished simply by closing the waveguide by introducing wall segments across the open side in those sections. A similar idea was adopted for an electric dipole array [26]. Several metal cavities were introduced to alternately enclose the aperture of a parallel strip line to achieve a high directivity OHP pattern. However, the aperture antenna in either case has wasted significant radiation area, i.e., they are much less efficient since their effective aperture area would be immediately decreased to only 2/3 of the physical aperture area. Hence, at the very best, they would only attain a 66.7% aperture efficiency.

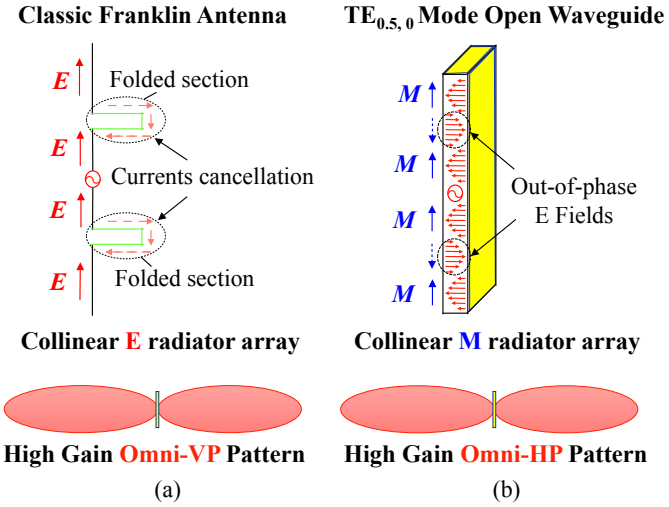

Fig. 1. High directivity omnidirectional array designs. (a) An electric dipole array (Franklin antenna). (b) A magnetic dipole array based on a $TE_{0.5,0}$ mode open waveguide.

The main innovation of this paper is to introduce phase inverters that are seamlessly integrated into the open waveguide at the half-wavelength phase changing points. The electric fields along the entire open aperture then become in-phase without blocking any portion of the radiating aperture. As a result, a collinear, in-phase magnetic dipole antenna array is realized that has both high directivity and high aperture radiation efficiency.

III. Compact, OHP Magnetic Dipole Antenna Arrays Facilitated by $TE_{0.5,0}$ Mode Open Waveguide with Seamlessly Integrated Phase Inverters

The design paradigm led to two optimized prototypes that confirmed their simulated performance characteristics.

A. Design of the $TE_{0.5,\,0}$ mode open waveguide with phase inverters seamlessly integrated into it

The $TE_{0.5,0}$ mode open waveguide configuration with the

integrated phase inverters is illustrated in Fig. 2. The open waveguide has the dimensions $L \times W \times H$. It is center-fed. The dielectric constant of the medium enclosed by the waveguide is ε_r. The waveguide is electrically long with $L = 2\lambda_0$ and two phase inverters are introduced at $\lambda_0/2$ from the feed point, thus establishing four magnetic dipole sections.

Each phase inverter is highly compact and easily integrated into the waveguide. In contrast to the design in [36] that required two slots etched on both surfaces of a SIW structure, each phase inverter shown in Fig. 2 consists of a single meandering slot that is etched in the top surface of the waveguide. This slot is surrounded by eight vias that short together the top and bottom surfaces of the waveguide and that are arranged in the indicated alternating pattern, being positioned next to the short sides of the slot, to achieve the desired phase inversion. Moreover, the single slot design also avoids an issue if one side of the waveguide needs to be employed as the ground for an external feed network.

The dimensions of the slot are defined as W_s, l_{s1}, l_{s2} in Fig. 2. The diameter of each shorting via is D_v and the distance between the centers of the two rows of vias in each inverter is d_v. Every two phase inverters, looking away from the center of the waveguide, are mirrored with respect to it. The distance between each pair is d_p. The distance of the feed from the open waveguide wall in its center plane is d_f. The entire configuration is highly compact and is readily fabricated with standard, low-cost PCB manufacturing technology.

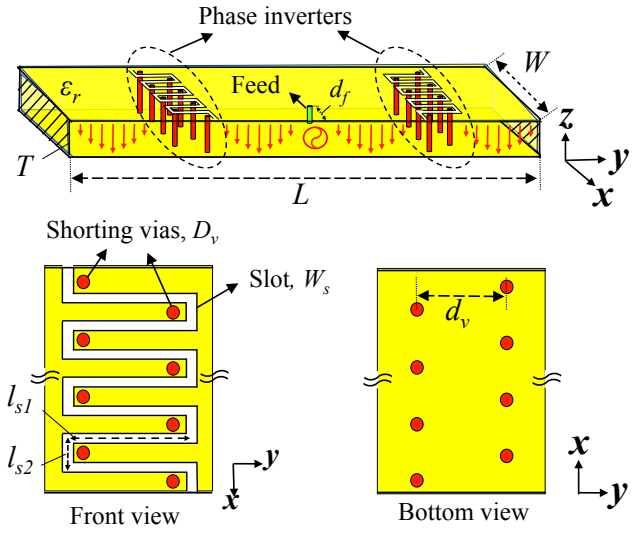

Fig. 2. Configuration of the $TE_{0.5,\,0}$ mode open waveguide with the phase inverters seamlessly integrated into it.

B. *Operating principles*

The phase inverters are the key to form the desired collinear and in-phase four-element magnetic dipole array. The sign of the electric fields inside a waveguide naturally changes when they propagate through each half-wavelength section away from the source. Each phase inverter is positioned to reverse this change.

This 180º phase reversal is accomplished by interrupting the current flow on the top and bottom surfaces of the waveguide. It is realized by cutting a meandered slot on the top surface and inserting plated vias on both sides (left and right) of it. This combination of the slot and vias facilitates the phase inversion of the electric fields as they propagate through it in the waveguide. An analogous phase inversion effect is reported in [37] for a balun design consisting of two parallel-strip lines, a slot and two vias. In our design, the slot-vias combination can be viewed as an a LC circuit. The shorting vias generate the inductance; the meandering slot produces the capacitance. This *LC* combination is optimized to act as a resonant bandpass filter that produces the desired 180˚ phase change. Because each phase inverter is composed of many individual elements, precise values of an equivalent circuit are not tenable. Nevertheless, both the simulated and measured results confirm that it is a very low loss structure. Guidelines for designing the phase inverter are given in the next subsection.

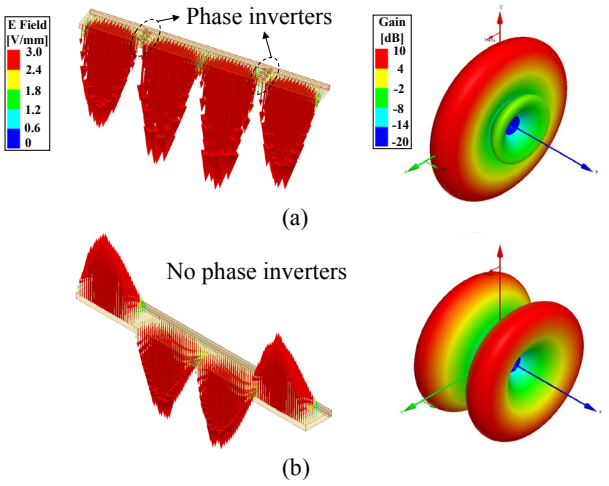

Fig. 3. Electric field distributions along the open aperture of the $TE_{0.5,0}$ mode waveguide with the source at its center and the corresponding radiation pattern it generates at the source frequency. (a) With the phase inverters. (b) Without the phase inverters.

Figure 3 shows the electric fields distribution along the aperture of the $TE_{0.5,\,0}$ mode center-fed open waveguide ($2\lambda_0$ long) with and without the phase inverters. It is clearly observed in Fig. 3(a) that the phase inverters effectively invert the electric fields as they pass through them. With the presence of the phase inverters, all of the electric fields (E-fields) along the aperture become in-phase. Thus, four collinear in-phase magnetic dipoles are achieved and an omni-directional pattern in the plane orthogonal to them will be generated. With the chosen axes and structure orientations, the high directivity, OHP radiation pattern will thus have its maximum in the $\varphi = 0^\circ$ plane. The peak omnidirectional gain for this four element array is 7.3 dBic. In contrast, the radiation pattern in Fig. 3(b) illustrates that the antenna without the integrated phase inverters generates a bi-conical beam pattern whose null is in the $\varphi = 0^\circ$ plane. The maximum directivity is pointing at $\theta = 30^\circ$ and the peak gain is 5.0 dBi. Given the E-field distributions and orientations, one could interpret the arrays as generating a sum (difference) pattern in Fig. 3(a) (Fig. 3(b)).

C. Key design considerations and guideline

Key design considerations of the OHP magnetic dipole array are presented. These include the dimension of the $TE_{0.5,0}$ mode open waveguide; the design of the phase inverter; the position of the feed; and the number of the magnetic dipole elements. Finally, a design guideline is developed from these discussions.

(a) Design of the $TE_{0.5,0}$ mode open waveguide

The main parameters of the $TE_{0.5,0}$ mode waveguide are the width W and length L of the waveguide and the relative permittivity of the dielectric filling it. With the open waveguide filled with Rogers™ 5880 substrate, the relative permittivity ε_r = 2.2. According to [38], the cutoff frequency f_{cutoff} of this waveguide mode and its phase constant k_g can then be determined by following equations:

$$f_{cutoff} = \frac{c}{4\sqrt{\varepsilon_r}\cdot W} \tag{1}$$

$$k_g = \sqrt{k_0^2\cdot\varepsilon_r - (\frac{\pi}{2W})^2} \tag{2}$$

It is clear that the width W of the waveguide determines the cutoff frequency.

To ensure that only the $TE_{0.5,0}$ mode propagates in the waveguide at X-band frequencies, the width W = 6.0 mm was chosen for the final design; it gives f_{cutoff} = 8.4 GHz. The wavelength in the waveguide is determined from the phase constant as $\lambda_g = 2\pi/k_g$. Given W = 6 mm, the calculated wavelength λ_g at 10 GHz is 37.6 mm. Then the total length of the four section case being considered will be near to $L = 2\lambda_g$. However, because of the presence of the phase inverters which have a finite length along the waveguide and their effect on the actual value of k_g, the final optimized length L of the four section waveguide is 68.0 mm.

The height H of the waveguide strongly affects the impedance of the antenna. The radiation resistance R_{rad} of the open waveguide will decrease if the height H becomes smaller. In particular, it becomes quite difficult to achieve good impedance matching if H is too small. Fig. 4(a) shows the real part of the input impedance of the antenna as functions of the source frequency for different heights H: 1.0, 1.28 and 1.58 mm. It is observed that the R_{rad} is less than 10 Ω around 10 GHz when the height H is as small as 1.0 mm, but increases to 25 Ω when H = 1.58 mm. The value H = 1.58 mm was selected for the final designs as it is one of the standard thicknesses of the Rogers™ 5880 substrate.

(b) Position of the feed

Another parameter that affects the antenna's input impedance is the position of the feed d_f. Fig. 4(b) presents the input impedance as a function of the source frequency for different d_f. It was found that the imaginary part of the impedance becomes smoother when the feed moves further away from the open face, deeper into the waveguide. A larger d_f also helps to increase the impedance bandwidth. The position of the feed must be adjusted carefully to achieve good impedance matching once H is determined. The value d_f = 3.4 mm is chosen for the final design.

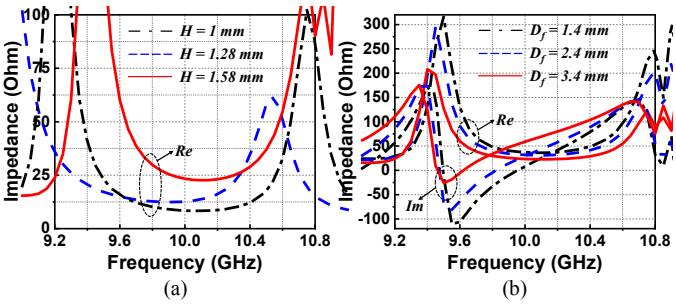

Fig. 4. Input impedance of the antenna as functions of the source frequency for (a) different heights of the waveguide, H; and (b) different feed positions d_f.

(c) Design of the phase inverter

It is critical to establish the proper inductance and capacitance values of the phase inverter that will minimize the reflections of the EM-waves passing through it. Fig. 3(a) illustrates the result of an optimized design. The field levels in each section are approximately equal. As noted previously, the inductance with the phase inverter is associated with the shorting vias. It is determined mainly by their diameter D_v and the height of the waveguide H. On the other hand, the capacitance of the phase inverter is determined mainly by the meandered slot and, hence, its design parameters: W_s, l_{s1}, and l_{s2}. Note that the distance d_v between the two rows of vias is only slightly smaller than l_{s1}. The structure looks like an interdigital capacitor [39] and is optimized with the following design parameter values: l_{s1} = 3.1 mm, l_{s2} = 0.85 mm, and W_s = 0.1 mm.

The effectiveness of the bandpass response of the phase inverter can be easily determined by monitoring the omnidirectional gain value in the φ = 0° plane at θ = 90°. A higher gain means the bandpass response is better. Fig. 5(a) presents it as a function of the source frequency for different distances d_v. It is observed that the omnidirectional gain is very poor around the targeted 10 GHz center frequency if all of the vias are in the same row (d_v = 0 mm). This outcome occurs because there is low interdigital capacitance so the resonance bandwidth is well above the desired frequencies. Fig. 5(b) clearly demonstrates that the phase inverters act as reflectors for this choice, yielding a very poor bandpass behavior, i.e., no fields reach the two outer sections. As Fig. 5(a) illustrates, the bandpass response is improved substantially as d_v is increased. The optimal value was found to be d_v = 1.0 mm for this design.

Once H is fixed, the inductance of the phase inverter is mainly determined by the diameter D_v of its shorting vias. Fig. 6(a) shows the gain values along the +z-axis, i.e., for φ = 0° and θ = 90°, as functions of the source frequency for different D_v. As expected, changing D_v causes the inductance to change, which then shifts the operating frequency band of the phase inverters. The peak gain of the antenna slightly increases when D_v becomes smaller which increases the inductance. Finally, D_v = 3.0 mm was chosen for the final design. It was a compromise choice between the maximum gain and the specified center

frequency, f_c = 10 GHz, of the operating band. Referring to [40], the inductance value of each shorting via is thus 1.2 nH. With properly designed meandered slot and shorting vias, the desired high directional omni-pattern shown in Fig. 6(b) was realized.

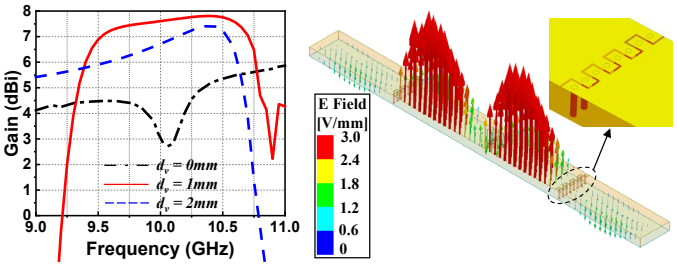

(a) (b)

Fig. 5. (a) Omnidirectional gain values as functions of the source frequency for different distance d_v between the two rows of the vias. (b) Electric field distribution along the aperture when the distance d_v = 0 mm.

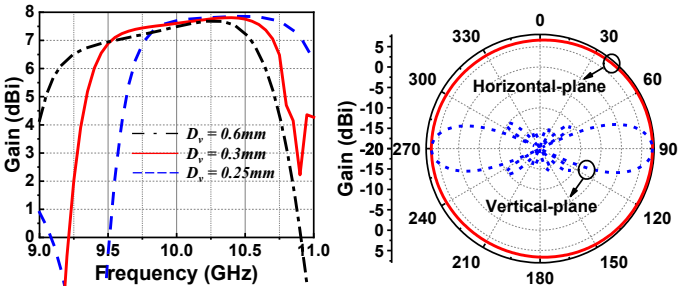

(a) (b)

Fig. 6. (a) Omnidirectional gain values as functions of the source frequency for different via diameters D_v. (b) Radiation patterns at the source frequency in both the omni- ($\varphi = 0^\circ$) and vertical- ($\theta = 90^\circ$) planes.

(d) Number of collinear magnetic dipoles

It should be expected that the maximum omni-directivity will increase if more elements are cascaded away from both sides of the source plane. As shown in Fig. 7 (a), OHP arrays with 2 to 10 magnetic dipole elements was studied. Fig. 7 (b) shows the gain values as functions of the source frequency as the number cascaded magnetic dipoles increases from 2 to 10 in steps of 2. It was found that the peak gain values are, respectively, 5.2, 7.8, 9.3, 10.4 and 11.4 dBi. On the other hand, the gain bandwidth decreases as the number of elements increases. For example, the 1.0-dB gain bandwidths are 12.3% (9.5 to 10.75 GHz) for 4 elements; 6.7% (10 to 10.7 GHz) for 6 elements; 4.8% (10.2 to 10.7 GHz) for 8 elements; and 3.3% (10.3 to 10.65 GHz) for 10 elements.

(e) Design guidelines

Design guidelines for arbitrary frequency operation can be extracted from the above discussions. Thanks to the resulting concise structure, the design process is easy and straightforward. The initial values of the dimensions (L, W and H) of the $TE_{0.5,0}$ mode waveguide are determined from the equations (1) and (2) and the material filling it. The initial dimension of the meandered slot can be obtained from [36]. The size of the shorting vias can be calculated from [40]. After the optimization of the radiation performance, a simple microstrip feedline can be designed and attached to the waveguide. Tuning stubs are used for good impedance matching, for instance, to a 50 Ω source. These feed issues are discussed below in detail relative to each realized prototype. Specific numbers of magnetic dipole elements can be adopted for diverse applications requiring a particular directivity value and bandwidth.

For example, the array designs with 2, 4, and 6 elements which are suitable for WLAN applications require larger radiation coverage with only medium directivity and sufficient bandwidth (>5%). On the other hand, higher directivity arrays with 8 or 10 elements are quite suitable for wireless power transfer applications [41], [42] that require higher directivities, but narrower bandwidths.

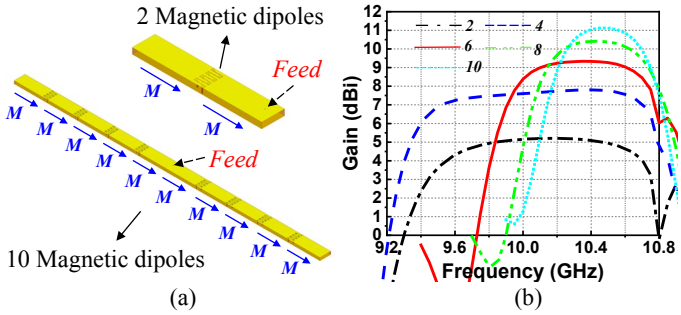

(a) (b)

Fig. 7. Collinear array of magnetic dipoles. (a) Configurations of the 2 and 10 element cases. (b) Gain of the array as a function of the source frequency as the number of dipoles increases.

D. Fabricated and tested six-element OHP array prototype

To verify these design guidelines, the consequent simulated performance characteristics and appropriate feeding mechanisms, arrays with 6 and 8 MD elements were optimized and tested.

(a) Single-feed six-element array design

The realization of the six-element magnetic dipole array is shown in Fig. 8. To implement its design with standard PCB manufacturing technology, the $TE_{0.5,0}$ mode waveguide is fabricated as a SIW structure. Recall that it is filled with the Rogers™ 5880 substrate that has a 1.575 mm thickness, a relative permittivity of 2.2, and a loss tangent of 0.0009 at 10 GHz. The thickness of the metallization layer is 17 μm (0.5 oz). The diameter D_{SIW} of each SIW via is 0.6 mm and the distance d_{SIW} between any two adjacent vias is 0.8 mm.

As shown in Fig. 8, a custom-designed compact microstrip feed line is fabricated on a much thinner (0.508 mm) sheet of Rogers™5880, substrate#2. It resides directly on the bottom of the waveguide. Its ground layer seamlessly touches on the bottom metallization layer of *Substrate#1*. While the array is center-fed, this feedline is driven with a SMA connector attached to the waveguide at one of its closed ends. The inner conductor of the SMA is connected to the 50-Ω transmission line on *Substrate#2* and the outer conductor of the SMA is

soldered to the bottom copper layer of *Substrate#1*. Good impedance matching is realized by introducing two impedance transformers and a tuning stub. The optimization process was conducted with the Keysight ADS (advanced design system) circuit simulator and the ANSYS HFSS (high frequency structure simulator) full-wave electromagnetics modeling software. The simulated input impedance of the short (length l_{f4}) 50-Ω transmission line connected to the feed probe at center of the waveguide was obtained with HFSS simulations. The resulting S1P data was then imported into ADS. Four sections of a transmission line model were constructed, e.g., a 50-Ω transmission line connected to the SMA, two impedance transformers and a tuning stub, were readily built and the optimized impedance bandwidth was obtained after quick manual tuning. A full-wave HFSS simulation model of the cascaded transmission line based on these optimized values was then built. The final optimization of this design was conducted in HFSS by slightly tuning the lengths of each portion of the transmission line to account for the radiation processes.

The detailed dimension of the optimized microstrip feed lines are: $l_{f1} = 24.7$ mm, $l_{f2} = 13.74$ mm, $l_{f3} = 8.98$ mm, $l_{f4} = 4.67$ mm, $l_{stub} = 3.44$ mm, $w_{50\Omega} = 1.56$ mm, $w_{stub} = 0.35$ mm, $w_t = 0.3$ mm. The array design parameters are listed in Table I. All of these parameters are noted in Fig. 8.

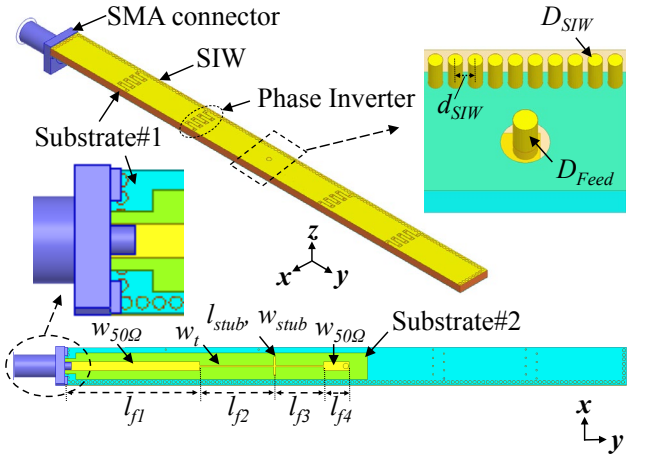

Fig. 8. Configuration of the six-element OHP magnetic dipole array prototype.

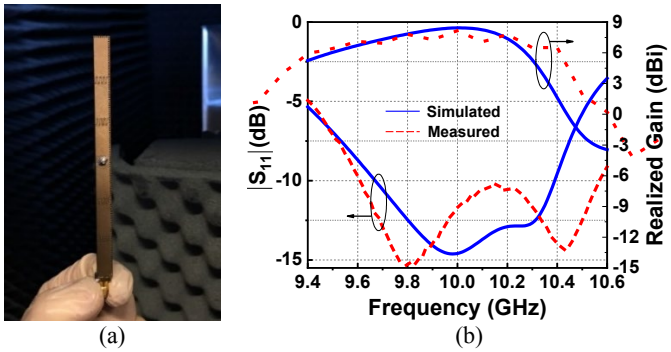

(a) (b)

Fig. 9. (a) Six-element OHP magnetic dipole array prototype fabricated with standard PCB manufacturing technology; and (b) Measured and simulated $|S_{11}|$ and realized gain values of the six-element OHP magnetic dipole array as functions of the source frequency.

TABLE I:
SIX-ELEMENT OHP MAGNETIC DIPOLE ARRAY DESIGN PARAMETERS
(DIMENSIONS IN MILLIMETERS)

Parameter	Description	Value
L	Length of the $TE_{0.5,0}$ mode waveguide	103.0
W	Width of the $TE_{0.5,0}$ mode waveguide	6.8
H	Height of the $TE_{0.5,0}$ mode waveguide	1.575
l_{s1}	Length of the meandered slot	3.1
W_s	Width of the meandered slot	0.1
D_v	Diameter of the shorting via	0.3
d_f	Distance of the feed to waveguide opening	3.4
d_{SIW}	Distance of adjunct SIW vias	0.8
D_{SIW}	Diameter of SIW vias	0.6
D_{Feed}	Diameter of the feed	1.0

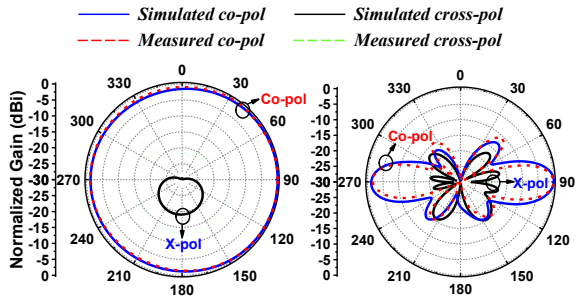

(a) Horizontal-pattern ($\phi = 0^\circ$) and Vertical-pattern ($\theta = 90^\circ$) at 9.6 GHz

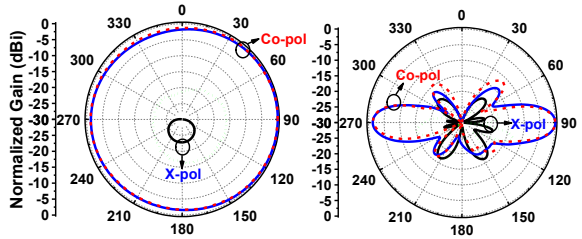

(b) Horizontal-pattern ($\phi = 0^\circ$) and Vertical-pattern ($\theta = 90^\circ$) at 9.8 GHz

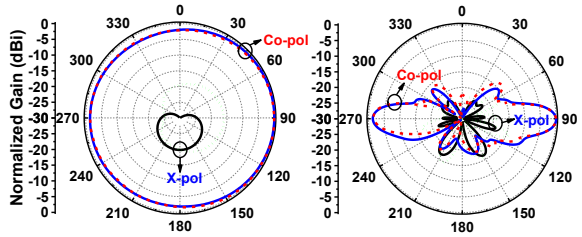

(c) Horizontal-pattern ($\phi = 0^\circ$) and Vertical-pattern ($\theta = 90^\circ$) at 10 GHz

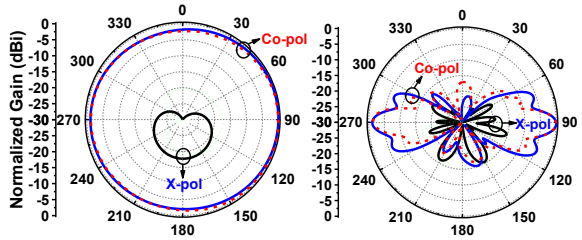

(d) Horizontal-pattern ($\phi = 0^\circ$) and Vertical-pattern ($\theta = 90^\circ$) at 10.2 GHz

Fig. 10. Measured and simulated normalized realized gain patterns of the six-element OHP magnetic dipole array in the horizontal plane, $\varphi = 0°$ (left), and in the vertical plane, $\theta = 90°$ (right) at 9.6, 9.8, 10.0 and 10.2 GHz.

(b) Measured results

The fabricated prototype is shown in Fig. 9 (a). It is highly compact, lightweight and low cost. The entire volume is only $0.07 \times 0.22 \times 3.3\ \lambda_0^3 = 0.051\ \lambda_0^3$. The $|S_{11}|$ values of the antenna were measured with a Keysight™ Vector Network Analyzer (VNA). Its radiation patterns were measured with a MVG far-field compact range system.

The measured and simulated $|S_{11}|$ and realized gain values as functions of the source frequency are compared in Fig. 9 (b). One observes that the measured results agree very well with their simulated values. The measured overlapping 10-dB impedance and 3-dB realized gain bandwidths is 800 MHz (8%), from 9.6 to 10.4 GHz. The measured peak realized gain value is 8.2 dBi.

The measured and simulated normalized realized gain patterns in both the horizontal and vertical planes are compared at 9.6, 9.8, 10, and 10.2 GHz in Fig. 10. The measured and simulated results agree reasonably well. The simulated radiation efficiency is above 95% over the operational bandwidth. The simulated overall antenna efficiency, i.e., the ratio of the total radiated power to the input power, at 9.6, 9.8, 10, and 10.2 GHz is 84%, 92%, 95%, and 93%, respectively. High directivity and omnidirectional HP fields were achieved within the entire operating band. The gain variation is less than 3 dB. The measured (simulated) out-of-roundness values of the omni-patterns are 1.9 dB (1.86 dB), 2 dB (2.2 dB), 2.3 dB (2.4 dB), and 2.4 dB (2.2 dB) at 9.6, 9.8, 10, and 10.2 GHz, respectively. The measured sidelobe levels are less than 10 dB within the entire operating band.

E. Fabricated and tested eight-element OHP array prototype

In order to enhance the directivity further while demonstrating that the operating bandwidth can be maintained, a center-fed eight-element OHP magnetic dipole array was developed. This two-element array consists of two four-element subarrays fed naturally by a single source. Recall from Fig. 7(b) that the operating bandwidth of the multi-element array becomes narrower as more elements are added. In contrast, this two-subarray antenna maintains the bandwidth *and* achieves a higher directivity. Consequently, its gain-bandwidth product is larger than an end-fed eight-element design. Moreover, it is feasible to expand this center-fed side-by-side design to even a larger scale with, for example, four or eight subarrays for yet higher omni-directivity.

(a) Array design

The realization of the eight-element magnetic dipole array is shown in Fig. 11. Similar to the single-feed six-element array, this design requires two pieces of the Rogers™ 5880 substrate. In contrast, it has two subarrays placed end-to-end where each subarray has its own excitation achieved with a 1 to 2 microstrip power divider feed network. The input port of the power divider is located at the center of the entire array. Considering the trace lengths and losses associated with a microstrip line feed network, the power divider is designed with the shortest possible total length to minimize those losses. Several sections of impedance transformers are adopted for good impedance matching to the 50-Ω source. The design procedure of the microstrip line feed network is similar to the 6-element design. It was conducted with ADS and HFSS co-simulations. The whole structure is still compact, lightweight and low cost. The detailed dimensions of the microstrip power divider feed network are: l_{f1} = 4.5 mm, l_{f2} = 15 mm, l_{f3} = 6 mm, l_{f4} = 6 mm, $w_{50\Omega}$ = 1.56 mm, w_{t1} = 0.35 mm, w_{t2} = 1.1 mm, w_{t3} = 0.44 mm. The array design parameters are listed in Table II.

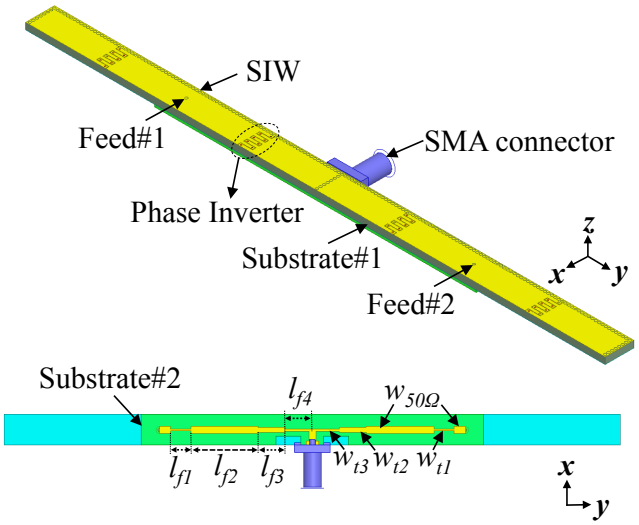

Fig. 11. Configuration of the eight-element OHP array prototype.

TABLE II:
EIGHT-ELEMENT OHP MAGNETIC DIPOLE ARRAY DESIGN PARAMETERS
(DIMENSIONS IN MILLIMETERS)

Parameter	Description	Value
L	Length of the $TE_{0.5,0}$ mode waveguide	137
W	Width of the $TE_{0.5,0}$ mode waveguide	6.8
H	Height of the $TE_{0.5,0}$ mode waveguide	1.575
l_{s1}	Length of the meandered slot	2.9
W_s	Width of the meandered slot	0.1
D_v	Diameter of the shorting via	0.3
d_f	Distance of the feed to waveguide opening	3.5
d_{SIW}	Distance of adjunct SIW vias	0.8
D_{SIW}	Diameter of SIW vias	0.6
D_{Feed}	Diameter of the feed	0.6

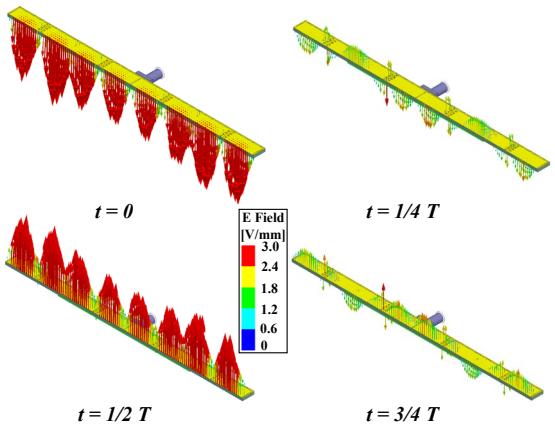

Fig. 12. Electric field distributions along the $TE_{0.5,0}$ mode waveguide at quarter period steps during one time period T of the 10 GHz source frequency.

The E-field distributions along this optimized eight-element array at quarter period steps in one time period of the 10 GHz source frequency are shown in Fig. 12. It is observed that all of the electric fields in each of the eight MD sections are in-phase and resonant in the same manner. Thus, eight collinear, in-phase magnetic dipoles were successfully achieved.

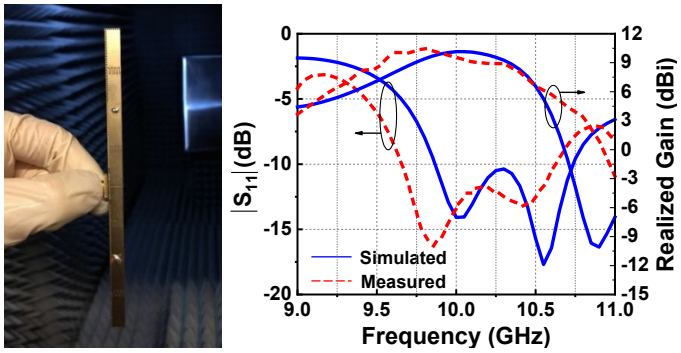

(a) (b)

Fig. 13. (a) Fabricated prototype of the eight-element OHP magnetic dipole array; and (b) Measured and simulated $|S_{11}|$ and realized gain values of the eight-element OHP magnetic dipole array as functions of the source frequency.

(b) Measured results

The fabricated prototype antenna is shown in Fig. 13 (a). The volume is only $0.07 \times 0.22 \times 4.3\ \lambda_0^3 = 0.066\ \lambda_0^3$. The measured and simulated $|S_{11}|$ and realized gain values as functions of the source frequency are compared in Fig. 13 (b). The measured and simulated results agree very well. The measured operating bandwidth shifts slightly lower. The measured overlapping 10-dB impedance and 3-dB realized gain bandwidth is 800 MHz (8%) from 9.6 to 10.4 GHz. It should be noted that the simulated 1-dB gain bandwidth of this eight-element design is 1.1GHz (11.2%) from 9.23 to 10.33 GHz. On the other hand, the simulated 1-dB gain bandwidth of the single-feed six-element design is only 0.56 GHz (5.6%) from 9.64 to 10.2 GHz. As might be expected from the six-element discussion, the gain bandwidth of a single-feed eight-element array would be smaller due to the presence of higher order modes. However, the prototype consists of two single-feed four-element sub-arrays, each of which has more gain bandwidth than the six-element case. Nevertheless, there is a limitation in this case on the impedance matching in the lower band due to the impedance bandwidth being narrower than the gain bandwidth. Consequently, the realized gain operating bandwidth of the two-feed eight element array remains 8%. The measured peak realized gain value is 10.4 dBi, achieving a RG per unit wavelength, 2.42 dBi/λ_0.

Fig. 14 shows the measured and simulated normalized realized gain patterns in both the horizontal and vertical planes at 9.8 GHz, 10 GHz and 10.2 GHz. The measurements and simulations agree reasonably well. Higher directivity was achieved as compared with the six-element design. The simulated radiation efficiency is again above 95% over the operational bandwidth. The simulated overall antenna efficiency at 9.8, 10, and 10.2 GHz is 85%, 96%, and 91%, respectively. Good omnidirectional patterns are observed

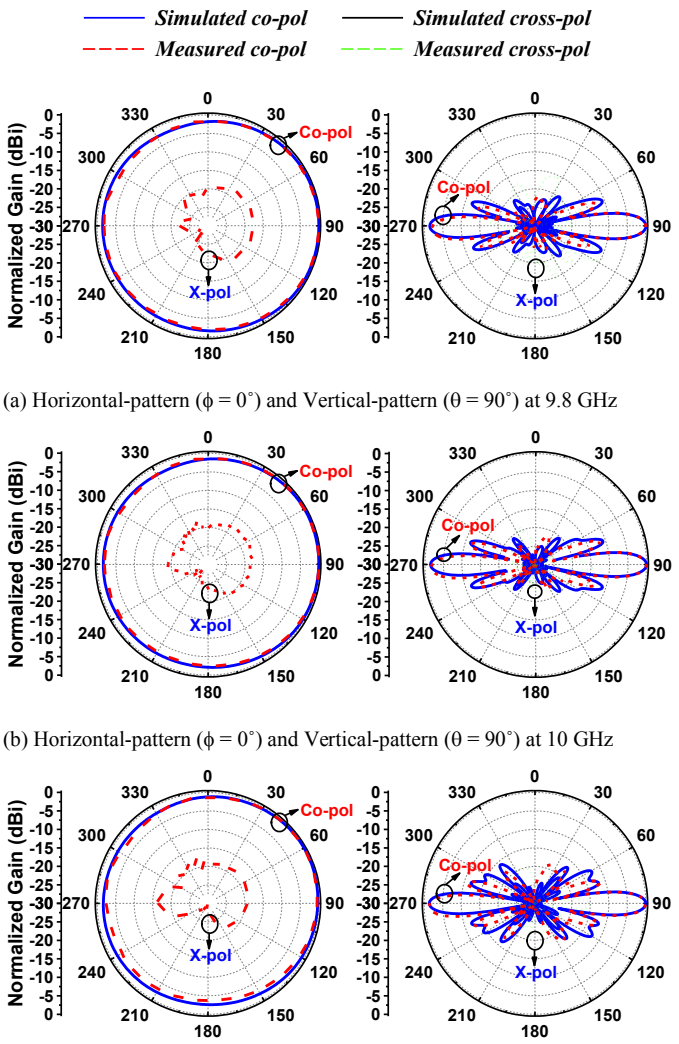

(a) Horizontal-pattern ($\phi = 0^\circ$) and Vertical-pattern ($\theta = 90^\circ$) at 9.8 GHz

(b) Horizontal-pattern ($\phi = 0^\circ$) and Vertical-pattern ($\theta = 90^\circ$) at 10 GHz

(c) Horizontal-pattern ($\phi = 0^\circ$) and Vertical-pattern ($\theta = 90^\circ$) at 10.2 GHz

Fig. 14. Measured and simulated normalized realized gain patterns of the eight-element OHP magnetic dipole array in the horizontal plane, $\varphi = 0^\circ$ (left), and in the vertical plane, $\theta = 90^\circ$ (right) at 9.6, 9.8, 10.0 and 10.2 GHz.

TABLE III:
PERFORMANCE COMPARISON OF HIGH DIRECTIVITY, OMNIDIRECTIONAL, HORIZONTALLY POLARIZED ANTENNA ARRAYS

Ref.	BW (%)	Peak RG (dBi)	Length (λ_0) and Total Size (λ_0^3)	Gain variation (dB) at f_c	RG per unit length (dBi/λ_0)
[26]	2	8.6	3.26, 0.445	1.94	2.64
[28]	1.5	3.87	2.6, 0.015	N.A.	1.49
[30]	7.3	9.7	6, 0.055	1.8	1.62
[27]	10.6	8.7	3.25, 1.47	2.1	2.68
[31]	34	8	7.1, 6.74	2	1.13
Developed 6-element design	**8**	**8.2**	**3.3, 0.051**	**2**	**2.48**
Developed 8-element design	**8**	**10.4**	**4.3, 0.066**	**2.7**	**2.42**

within the entire operation band. The measured (simulated) out-of-roundness values of the omni-patterns are 2.6 dB (2.3 dB), 2.7 dB (2.3 dB), and 3.5 dB (2.7 dB), at 9.8, 10.0, and 10.2 GHz, respectively. The measured out-of-roundness values are

slightly larger than the simulated results due to misalignments in the measurement setup. The accurate alignment becomes more difficult if the antenna under test is longer. Note that all the simulated out-of-roundness values are less than 3 dB within the operating bandwidth. The measured sidelobe levels are less than 10 dB within the entire bandwidth.

IV. Conclusions

The design paradigm, the corresponding operating principles, and measurement results prototypes of two high directivity, compact, omnidirectional horizontally polarized (OHP) magnetic dipole antenna arrays were reported. As summarized in Table III, they achieved outstanding performance characteristics when compared to all of the reported OHP antenna arrays to date (to the best of our knowledge). For instance, the achieved 8% bandwidth for both designs is much larger than those in [26] and [28], 2.0% and 1.5%, respectively. The design in [30] achieved a comparable bandwidth, 7.3%, but the structure is much longer. The realized gain per unit length of the waveguide aperture (1.62 dBi) is much lower than our developed designs (2.48 dBi for the six-element and 2.42 dBi for the eight-element designs). The antenna in [27] has a higher bandwidth (10.6%) and comparable realized gain per unit length (2.68 dBi). However, the entire volume is 1.47 λ_0^3, which is 29 times larger than our six-element design (0.05 λ_0^3). Moreover, the fabrication and implementation processes are much more complicated. The design in [31] achieved a larger bandwidth (34%). Nonetheless, its entire volume is large, 6.74 λ_0^3, which is more than 134 times larger than our reported six-element design (0.05 λ_0^3 volume) and yields a slightly lower peak realized gain.

In summary, the OHP magnetic dipole antenna arrays developed in this work are the first that achieve simultaneously a compact in size; a light weight; a low cost, concise design ; high directivity, and wide bandwidth. They are ideal candidates for wireless applications that require high directivity OHP performance characteristics.

V. Acknowledgements

The authors would like to thank Dr. Shulin Chen and Mr. Jiwei Lian, University of Technology Sydney, Prof. Zheng Li, Beijing Jiaotong University, for valuable discussions; and Prof. Y. Jay Guo, University of Technology Sydney, for his support of these efforts.

References

[1] B. Li, S. W. Liao, and Q. Xue, "Omnidirectional circularly polarized antenna combining monopole and loop radiators," *IEEE Antennas Wirel. Propag. Lett.*, vol. 12, pp. 607–610, 2013.

[2] Y. M. Pan and K. W. Leung, "Wideband omnidirectional circularly polarized dielectric resonator antenna with parasitic strips*," IEEE Trans. Antennas Propag.*, vol. 60, no. 6, pp. 2992-2997, Jun. 2012.

[3] K.-L. Wong, F.-R. Hsiao, and T.-W. Chiou, "Omnidirectional planar dipole array antenna," *IEEE Trans. Antennas Propag.*, vol. 52, no. 2, pp. 624–628, Feb. 2004.

[4] W. Lin, R. W. Ziolkowski, and T. C. Baum, "28 GHz compact omnidirectional circularly polarized antenna for Device-to-Device communications in the future 5G systems," *IEEE Trans. Antennas Propag.*, vol. 65, no. 12, pp. 6904-6914, Dec. 2017.

[5] H. Huang, Y. Liu, and S. Gong, "Broadband dual-polarized omnidirectional antenna for 2G/3G/LTE/WiFi applications," *IEEE Antennas Wireless Propag. Lett.*, vol. 15, pp. 576–579, 2016.

[6] D. Chizhik, J. Ling, and R. A. Valenzuela, "The effect of electric field polarization on indoor propagation," in *Proc. IEEE Int. Conf. Universal Pers. Commun. (ICUPC)*, vol. 1. Oct. 1998, pp. 459–462.

[7] Y. Li, Z. Zhang, Z. Feng, and M. F. Iskander, "Design of omnidirectional dual-polarized antenna in slender and low-profile column," *IEEE Trans. Antennas Propag.*, vol. 62, no. 4, pp. 2323-2326, Apr. 2014.

[8] Y. Li, Z. Zhang, J. Zheng, and Z. Feng, "Compact azimuthal omnidirectional dual-polarized antenna using highly isolated colocated slots," *IEEE Trans. Antennas Propag.*, vol. 60, no. 9, pp. 4037–4045, Sep. 2012.

[9] A. Alford and A. G. Kandoian, "Ultrahigh-frequency loop antennas," *Elect. Eng.*, vol. 59, no. 12, pp. 843–848, Dec. 1940.

[10] Y. Yu, F. Jolani, and Z. Chen, "A wideband omnidirectional horizontally polarized antenna for 4G LTE applications," *IEEE Antennas Wireless Propag. Lett.*, vol. 12, pp. 686–689, 2013.

[11] C. H. Ahn, S. W. Oh, and K. Chang, "A dual-frequency omnidirectional antenna for polarization diversity of MIMO and wireless communication applications," *IEEE Antennas Wireless Propag. Lett.*, vol. 8, pp. 966–969, 2009.

[12] C. C. Lin, L. C. Kuo, and H. R. Chuang, "A horizontally polarized omnidirectional printed antenna for WLAN applications," *IEEE Trans. Antennas Propag.*, vol. 54, no. 11, pp. 3551–3556, Dec. 2006.

[13] K. Wei, Z. Zhang, and Z. Feng, "Design of a wideband horizontally polarized omnidirectional printed loop antenna," *IEEE Antennas Wireless Propag. Lett.*, vol. 11, pp. 49–52, 2012.

[14] Q. Liu, Y. Yu, and S. He, "Capacitively loaded, inductively coupled fed loop antenna with an omnidirectional radiation pattern for UHF RFID tags," *IEEE Antennas Wireless Propag. Lett.*, vol. 12, pp. 1161–1164, 2013.

[15] X. Qing and Z. N. Chen, "Horizontally polarized omnidirectional segmented loop antenna," in *Proc. 6th Eur. Conf. Antennas Propag. (EUCAP)*, Mar. 2011, pp. 2904–2907.

[16] X. Qing, C. K. Goh, and Z. N. Chen, "A broadband UHF near-field RFID antenna," *IEEE Trans. Antennas Propag.*, vol. 58, no. 12, pp. 3829–3838, Dec. 2010.

[17] L. Sun, Y. Li, Z. Zhang, and M. F. Iskander, "A compact planar omnidirectional MIMO array antenna with pattern phase diversity using folded dipole element," *IEEE Trans. Antennas Propag.*, vol. 67, no. 3, pp. 1688– 1696, Mar. 2019.

[18] J. Wang, L. Zhao, Z. C. Hao, and J.M. Jin, "A wideband dual-polarized omnidirectional antenna for base station/WLAN," *IEEE Trans. Antennas Propag.*, vol. 66, no. 1, pp. 81–87, Jan. 2018.

[19] J. Wang, Z. Shen, and L. Zhao, "Wideband dual-polarized antenna for spectrum monitoring systems," *IEEE Antennas Wireless Propag. Lett.*, vol. 16, pp. 2236–2239, 2017.

[20] K. Fan, Z.-C. Hao, Q. Yuan, J. Hu, G. Q. Luo, and W. Hong, ''Wideband horizontally polarized omnidirectional antenna with a conical beam for millimeter-wave applications,'' *IEEE Trans. Antennas Propag.,* vol. 66, no. 9, pp. 4437–4448, Sep. 2018.

[21] Z. Y. Zhang, Y. Zhao, S. Zuo, L. Yang, L. Y. Ji, and G. Fu, "A broadband horizontally polarized omnidirectional antenna for VHF application," *IEEE Trans. Antennas Propag.,* vol. 66, no. 5, pp. 2229–2235, May 2018.

[22] X. Z. Cai and K. Sarabandi, "A compact broadband horizontally polarized omnidirectional antenna using planar folded dipole elements," *IEEE Trans. Antennas Propag.*, vol. 64, no. 2, pp. 414–422, Feb. 2016.

[23] H.-Y. Zhang, F.-S. Zhang, F. Zhang, T. Li, and C. Li, "Bandwidth enhancement of a horizontally polarized omnidirectional antenna by adding parasitic strips," *IEEE Antennas Wireless Propag. Lett.*, vol. 16, pp. 880–883, Feb. 2017.

[24] Y. Fan, X. Liu, B. Liu, and R.-L. Li, "A broadband dual-polarized omnidirectional antenna based on orthogonal dipoles," *IEEE Antennas Wireless Propag. Lett.*, vol. 15, pp. 1257–1260, 2016.

[25] Z. D. Wang, Y. Z. Yin, X. Ying and J. J. Wu, "Design of a wideband horizontally polarized omnidirectional antenna with mutual coupling method," *IEEE Trans. Antennas Propag.*, vol. 63, no. 7, pp. 3311–3316, Jul. 2015.

[26] L. Chang, Y. Li, Z. Zhang and Z. Feng, "Horizontally polarized omnidirectional antenna array using cascaded cavities," *IEEE Trans. Antennas Propag.*, vol. 64, no. 12, pp. 5454–5459, 2016.

[27] K. Wei, Z. Zhang, Z. Feng and M. F. Iskander, "A MNG-TL loop antenna array with horizontally polarized omnidirectional patterns," *IEEE Trans. Antennas Propag.*, vol. 60, no. 6, pp. 2702–2710, 2012.
[28] G. Hua, W. Hong, X. H. Sun, and H. X. Zhou, "Design of an omnidirectional line array with SIW longitudinal slot antenna," in *Proc. ICMMT*, Apr. 2008, pp. 1114–1117.
[29] Z. Zeng et al., "The design and experiment of a dual-band omnidirectional SIW slot array antenna," in *Proc. APMC*, Bangkok, Thailand, Dec. 2007, pp. 1–4.
[30] Z. Liang, Y. Li, X. Feng, J. Liu, J. Qin, and Y. Long, "Microstrip magnetic monopole and dipole antennas with high directivity and a horizontally polarized omnidirectional pattern," *IEEE Trans. Antennas Propag.*, vol. 66, no. 3, pp. 1143–1152, Mar. 2018.
[31] X. L. Quan, R. L. Li, J. Y. Wang, and Y. H. Cui, "Development of a broadband horizontally polarized omnidirectional planar antenna and its array for base stations," *Prog. Electromagn. Res.*, vol. 128, pp. 441–456, Jun. 2012.
[32] K. P. Wei, Z. J. Zhang, Z. H. Feng, and M. F. Iskander, "Periodic leaky-wave antenna array with horizontally polarized omnidirectional pattern," *IEEE Trans. Antennas Propag.*, vol. 60, no. 8, pp. 3165–3173, Aug. 2012.
[33] N. Nguyen-Trong, T. Kaufmann, and C. Fumeaux, "A wideband omnidirectional horizontally polarized traveling-wave antenna based on half-mode substrate integrated waveguide," *IEEE Antennas Wireless Propag. Lett.*, vol. 12, pp. 682–685, 2013.
[34] W. Lin, R. W. Ziolkowski and J. Q. Huang, "Electrically small, low profile, highly efficient, Huygens dipole rectennas for wirelessly powering Internet-of-Things (IoT) devices," *IEEE Trans. Antennas Propag*., vol. 67, no. 6, pp. 3670-3679, June. 2019.
[35] C. S. Franklin, "Improvements in wireless telegraph and telephone aerials," *British Patent* 242342, Aug. 1914.
[36] X. Zou, F. Z. Geng, Y. Li, and Y. Leng, ''Phase inverters based on substrate integrated waveguide,'' *IEEE Microw. Wireless Compon. Lett.*, vol. 27, no. 3, pp. 227–229, Mar. 2017.
[37] J. T. Zeng and K. M. Luk, "Wideband millimeter-wave end-fire magneto-electric dipole antenna with microstrip-line feed," *IEEE Trans. Antennas Propag.*, *in early access*. DOI: 10.1109/TAP.2019.2957089.
[38] Q. Lai, C. Fumeaux, W. Hong, and R. Vahldieck, "Characterization of the propagation properties of the half-mode substrate integrated waveguide," *IEEE Trans. Microw. Theory Tech.*, vol. 57, no. 8, pp. 1996–2004, Aug. 2009.
[39] G. D. Alley, "Interdigital capacitors and their application to lumped element microwave integrated circuits," *IEEE Trans. Microwave Theory Tech*., vol.18, no. 12, pp. 1028–1033, Dec. 1970.
[40] S. L. Chen, D. K. Karmokar, Z. Li, P. Y. Qin, R. W. Ziolkowski, and Y. J. Guo, "Circular-polarized substrate-integrated-waveguide leaky-wave antenna with wide-angle and consistent-gain continuous beam scanning," *IEEE Trans. Antennas Propag.*, vol. 67, no. 7, pp. 4418-4428, Jul. 2019.
[41] W. Lin and R. W. Ziolkowski, "Electrically small Huygens CP rectenna with a driven loop element maximizes its wireless power transfer efficiency," *IEEE Trans. Antennas Propag.*, vol. 68, no. 1, pp. 540-545, Jan. 2020.
[42] W. Lin and R. W. Ziolkowski, "Wirelessly powered temperature and light detecting sensors based on electrically small Huygens antennas," *Sensors*, vol. 19, no. 9, Apr. 2019.